The Anomalous Hall Effect and Magnetic Monopoles in Momentum Space

Zhong Fang *et al.*

Science **302**, 92 (2003);
DOI: 10.1126/science.1089408

which is much larger than the lattice spacing (or the Fermi wavelength). Here, the Mott insulator can be thought of as a state in which holes and doubly occupied sites form bound states due to their Coulomb interaction. The spatial extension ξ of these bound states is related to their energy (the Mott gap Δ) by $\Delta \sim h^2/(2m\xi^2)$. Given the measured value of Δ in samples close to the transition, this leads to the conclusion that ξ is indeed a large length scale, of order a few nanometers. Finally, we emphasize that our results provide experimental support to the early idea of (*12*) and to recent theories of the Mott critical endpoint based on the DMFT approach (*13*–*15*). Although further effort should be devoted to the inclusion of lattice degrees of freedom in these theories, simplified treatments of these effects (*16*) do emphasize the key role of electronic degrees of freedom in the transition.

References and Notes

1. N. F. Mott, *Proc. Phys. Soc. A* **62**, 416 (1949).
2. N. F. Mott, *Metal Insulator Transitions* (Taylor and Francis, London. 1990).
3. M. Imada, A. Fujimori, Y. Tokura, *Rev. Mod. Phys.* **70**, 1039 (1998).
4. D. B. McWhan, J. P. Remeika, *Phys. Rev. B* **2**, 3734 (1970).
5. A. Jayaraman, D. B. McWhan, J. P. Remeika, P. D. Dernier, *Phys. Rev. B* **2**, 3751 (1970).
6. D. B. McWhan *et al.*, *Phys. Rev. Lett.* **27**, 941 (1971).
7. D. B. McWhan, A. Menth, J. P. Remeika, W. F. Brickman, T. M. Rice, *Phys. Rev. B* **7**, 1920 (1973).
8. H. Kuwamoto, J. M. Honig, J. Appel, *Phys. Rev. B* **22**, 2626 (1980).
9. H. Harrison, R. Aragon, C. J. Sandberf, *Mater. Res. Bull.* **15**, 571 (1980).
10. A. Kerlin, H. Nagasawa, D. Jérome, *Solid State Comm.* **13**, 1125 (1973).
11. L. Kadanoff *et al.*, *Rev. Mod. Phys.* **39**, 395 (1967).
12. C. Castellani, C. DiCastro, D. Feinberg, J. Ranninger, *Phys. Rev. Lett.* **43**, 1957 (1979).
13. G. Kotliar, E. Lange, M. J. Rozenberg, *Phys. Rev. Lett.* **84**, 5180 (2000).
14. M. J. Rozenberg, R. Chitra, G. Kotliar, *Phys. Rev. Lett.* **83**, 3498 (1999).
15. A. Georges, G. Kotliar, W. Krauth, M. J. Rozenberg, *Rev. Mod. Phys.* **68**, 13 (1996).
16. P. Majumdar, H. R. Krishnamurthy, *Phys. Rev. Lett.* **73**, 1525 (1994).

17. We acknowledge fruitful discussions with R. Chitra, S. Florens, G. Kotliar, H. R. Krishnamurthy, M. Rozenberg, and A. J. Millis.

Supporting Online Material

www.sciencemag.org/cgi/content/full/302/5642/89/DC1
Figs. S1 to S3

24 June 2003; accepted 20 August 2003

The Anomalous Hall Effect and Magnetic Monopoles in Momentum Space

Zhong Fang,[1,2]* Naoto Nagaosa,[1,3,4] Kei S. Takahashi,[5] Atsushi Asamitsu,[1,6] Roland Mathieu,[1] Takeshi Ogasawara,[3] Hiroyuki Yamada,[3] Masashi Kawasaki,[3,7] Yoshinori Tokura,[1,3,4] Kiyoyuki Terakura[8]

Efforts to find the magnetic monopole in real space have been made in cosmic rays and in particle accelerators, but there has not yet been any firm evidence for its existence because of its very heavy mass, $\sim 10^{16}$ giga–electron volts. We show that the magnetic monopole can appear in the crystal momentum space of solids in the accessible low-energy region ($\sim$0.1 to 1 electron volts) in the context of the anomalous Hall effect. We report experimental results together with first-principles calculations on the ferromagnetic crystal $SrRuO_3$ that provide evidence for the magnetic monopole in the crystal momentum space.

Dirac (*1*) postulated in 1931 the existence of a magnetic monopole (MM), searching for the symmetry between the electric and magnetic fields in the law of electromagnetism. A singularity in the vector potential is needed for this Dirac MM to exist. Theoretically, the MM was found (*2*, *3*) as the soliton solution to the equation of the non-Abelian gauge theory for grand unification. However, its energy is estimated to be extremely large, $\sim 10^{16}$ GeV, which makes its experimental observation difficult. In contrast to this MM in real space, one can consider its dual space, namely, the crystal momentum (**k**-) space of solids, and the Berry phase connection (*4*) of Bloch wave functions. This MM in momentum space (*5*) is closely related to the physical phenomenon of the anomalous Hall effect (AHE) observed in ferromagnetic metals.

The AHE is a phenomenon in which the transverse resistivity (ρ_{xy}) in ferromagnets contains a contribution from the magnetization (M) in addition to the usual Hall effect. The conventional expression for ρ_{xy} is

$$\rho_{xy} = R_0 B + 4\pi R_s M \qquad (1)$$

where B is the magnetic field, R_0 is the usual Hall coefficient, and R_s is the anomalous Hall coefficient. This expression implicitly assumes that the additional contribution is proportional to M, and it is used as an experimental tool to measure M as a function of temperature. This analysis is extensively used in studies of ferromagnetic semiconductors with dilute magnetic impurities, which are the most promising materials for applications in spintronics (*6*). However, the mechanism of AHE has long been controversial (*7*–*11*). The key issues are whether the effect is intrinsic or extrinsic and how to treat the impurity and phonon scatterings. Karplus and Luttinger (*7*) were the first to propose the intrinsic mechanism of AHE, in which the matrix elements of the current operators are essential. Other theories (*8*, *11*) attribute the AHE to the impurity scattering modified by the spin-orbit interaction, namely, the skew scattering (*8*) and/or the side-jump mechanism (*11*). These extrinsic mechanisms are rather complicated and depend on the details of the impurities as well as on the band structure of the materials. Nevertheless, all these conventional theories (*7*–*11*) for the AHE derive Eq. 1, as they are based on the perturbative expansion of the spin-orbit coupling (SOC) λ and M; i.e., $R_s \propto \lambda$.

Recently, the geometrical meaning of the intrinsic-origin AHE (*6*) has been recognized (*12*–*15*). The transverse conductivity (σ_{xy}) can be written as the integral of the Berry phase curvature (the gauge field) over the occupied electronic states in crystal momentum space (Eq. 5). The MM corresponds to the source or sink of the gauge field or curvature defined by this Berry phase connection. Therefore, the AHE can be a direct fingerprint of the MM in crystal momentum space. The presence of time-reversal symmetry results in $\sigma_{xy} = \rho_{xy} = 0$ in the dc limit from the generic argument, and the group theoretical condition for the nonzero σ_{xy} is equivalent to that of finite ferromagnetic moment (supporting online text). Therefore, ferromagnets are neces-

[1]Spin Superstructure Project, Exploratory Research for Advanced Technology (ERATO), Japan Science and Technology Corporation, National Institute of Advanced Industrial Science and Technology (AIST), Tsukuba Central 4, Tsukuba 305-8562, Japan. [2]Institute of Physics, Chinese Academy of Science, Beijing 100080, China. [3]Correlated Electron Research Center, AIST Tsukuba Central 4, Tsukuba 305-8562, Japan. [4]Department of Applied Physics, University of Tokyo, 7-3-1 Hongo, Bunkyo-ku, Tokyo 113-8656, Japan. [5]Department of Condensed Matter Physics, University of Geneva, 24, quai Ernest-Ansermet, 1211 Geneva 4, Switzerland. [6]Cryogenic Center, University of Tokyo, 2-11-16 Bunkyo-ku, Tokyo 113-0032, Japan. [7]Institute for Materials Research, Tohoku University, Sendai 980-8577, Japan. [8]Research Institute for Computational Sciences, AIST Tsukuba Central 2, Tsukuba 305-8568, Japan.

*To whom correspondence should be addressed. E-mail: z.fang@aist.go.jp

sary to study σ_{xy}, even though the Berry phase connection is more universal and exists even in nonmagnetic materials.

We show by detailed first-principles band calculations combined with transport, optical, and magnetic measurements that the observed unconventional behavior of the AHE and Kerr rotation in the metallic ferromagnet $SrRuO_3$ is of intrinsic origin and is determined by the existence of a MM in **k**-space. The conventional expression (Eq. 1) is not supported by our experimental data, which show a nonmonotonous temperature dependence that even includes a sign change.

$SrRuO_3$ with perovskite structure is an itinerant (metallic) ferromagnet. Ru^{4+} has four t_{2g} electrons with low spin configurations. The 4*d* orbitals of $SrRuO_3$ are relatively extended and the bandwidth is large compared with its Coulombic interaction. The relativistic SOC is also large in its 4*d* electrons, because of the heavy atomic mass (on the order of 0.3 eV for the Ru atom). High-quality single crystal is now available with a residual resistivity on the order of 10 μΩcm. These aspects make this system an ideal candidate in which to observe the AHE due to the **k**-space gauge field. Stoichiometric $SrRuO_3$ (bulk and thin film) and Ca-doped ($Sr_{0.8}Ca_{0.2}RuO_3$ thin film) single crystals were prepared (*16*). The *M* curve (Fig. 1) of $SrRuO_3$ film is quite similar to that of bulk single crystal, except that the Curie temperature (T_c, ~150 K) is slightly lower than that of bulk (~160 K), because of the strain effects. However, the isovalent Ca-doping markedly suppresses T_c and *M*. All of the samples were used for transport measurements in the dc limit. As seen from Fig. 1C, the ρ_{xy} changes nonmonotonously with temperature and even includes a sign change. Such behavior is far beyond the expectation based on the conventional expression in Eq. 1. In addition to the transport measurement, the frequency (ω)–dependent conductivities (Fig. 2) were measured for $SrRuO_3$ film by an optical method (*16*). In addition to the strong structures around 3.0 eV, which are mostly due to the charge transfer from O-2*p* to Ru-4*d*, sharp structures were also observed for both the real and the imaginary part of $\sigma_{xy}(\omega)$ below 0.5 eV. These low-energy sharp structures cannot be fitted by extended Drude analysis. The lower the energy is, the stronger the deviations from fitting are. We will show, by combination with first-principles calculations, that these unconventional behaviors actually originate from the singular behavior of MMs in momentum space.

We now turn to some details of the theoretical analysis. The Berry phase is the quantal phase acquired by the wave function that is associated with the adiabatic change of the Hamiltonian (*4*, *17*). Let $|n(\boldsymbol{\alpha})\rangle$ be the *n*th eigenstate of the Hamiltonian $H(\boldsymbol{\alpha})$, with $\boldsymbol{\alpha} = (\alpha_1, \ldots, \alpha_m)$ being the set of parameters. The Berry's connection is the overlap of the two wave functions infinitesimally separated in $\boldsymbol{\alpha}$-space, i.e.

$$\langle n(\boldsymbol{\alpha})|n(\boldsymbol{\alpha}+\Delta\boldsymbol{\alpha})\rangle = 1+\Delta\boldsymbol{\alpha}\langle n(\boldsymbol{\alpha})|\nabla_{\alpha}|n(\boldsymbol{\alpha})\rangle = \exp[-i\Delta\boldsymbol{\alpha}\cdot\mathbf{a}_n(\boldsymbol{\alpha})] \quad (2)$$

where the vector potential $\mathbf{a}_n(\boldsymbol{\alpha})$ is defined by $\mathbf{a}_n(\boldsymbol{\alpha}) = i\langle n(\boldsymbol{\alpha})|\nabla_{\alpha}|n(\boldsymbol{\alpha})\rangle$. Although the concept of the Berry phase has broad applications in physics (*17*), its relevance to the band structure in solids has been recognized only recently and in limited situations, such as the quantum Hall effect under a strong magnetic field (*18*) and the calculation of electronic polarization in ferroelectrics (*19*, *20*). In this case, the parameter $\boldsymbol{\alpha}$ is the crystal momentum **k**. For the Bloch wave function $\psi_{n\mathbf{k}}(\boldsymbol{r}) = e^{i\mathbf{k}\cdot\mathbf{r}}u_{n\mathbf{k}}(\boldsymbol{r})$, where *n* denotes the band index and $u_{n\mathbf{k}}$ is the periodic part, the vector potential for the Berry phase $a_{n\mu}(\boldsymbol{k})$ is

$$a_{n\mu}(\boldsymbol{k}) = i\langle u_{n\mathbf{k}}|\frac{\delta}{\delta\mathbf{k}_{\mu}}u_{n\mathbf{k}}\rangle \quad (3)$$

where μ is the chemical potential. With this vector potential, the gauge covariant position operator x_{μ} for the wave packet made out of the band *n* is given by $x_{\mu} = i\partial_{k_{\mu}} - a_{n\mu}(\mathbf{k})$. Therefore, the commutation relation between x_{μ} and x_{ν} includes the gauge field $F_{\mu\nu} = \partial_{k_{\mu}}a_{n\nu} - \partial_{k_{\nu}}a_{n\mu}$, as

$$[x_{\mu}, x_{\nu}] = -iF_{\mu\nu} \quad (4)$$

which leads to the additional (anomalous) velocity $-i[x_{\mu}, V(x)] = -F_{\mu\nu}\partial V(x)/\partial x_{\nu}$, being transverse to the electric field $E_{\nu} = -\partial V(x)/\partial x_{\nu}$. Therefore, the transverse conductivity σ_{xy} is given by the sum of this anomalous velocity over the occupied states as (*18*)

$$\sigma_{xy} = \sum_{n,\mathbf{k}} n_F[\varepsilon_n(\mathbf{k})]b_z(\mathbf{k}) \quad (5)$$

where $b_z(\mathbf{k}) = F_{xy}(\mathbf{k})$, ε is $\varepsilon_n(\mathbf{k})$ is the eigen energy of $\Psi_{n\mathbf{k}}(\mathbf{r})$, β is the inverse temperature, and $n_F[\varepsilon] = 1/(e^{\beta(\varepsilon-\mu)} + 1)$ is the Fermi distribution function. Hence, the behavior of gauge field $b_z(\mathbf{k})$ in **k**-space (*21*) determines that of σ_{xy}. One might imagine that it is a slowly varying function of **k**, but that is not the case. Fig. 3B is the calculated result for $b_z(\mathbf{k})$ in the real system $SrRuO_3$. It has a very sharp peak near the Γ-point and ridges along the diagonals. The origin for this sharp structure is the (near) degeneracy and/or the band crossing, which act as MMs. Consider the general case where the two-band Hamiltonian matrix $H(\mathbf{k})$ at **k** can be written as $H(\mathbf{k}) =$

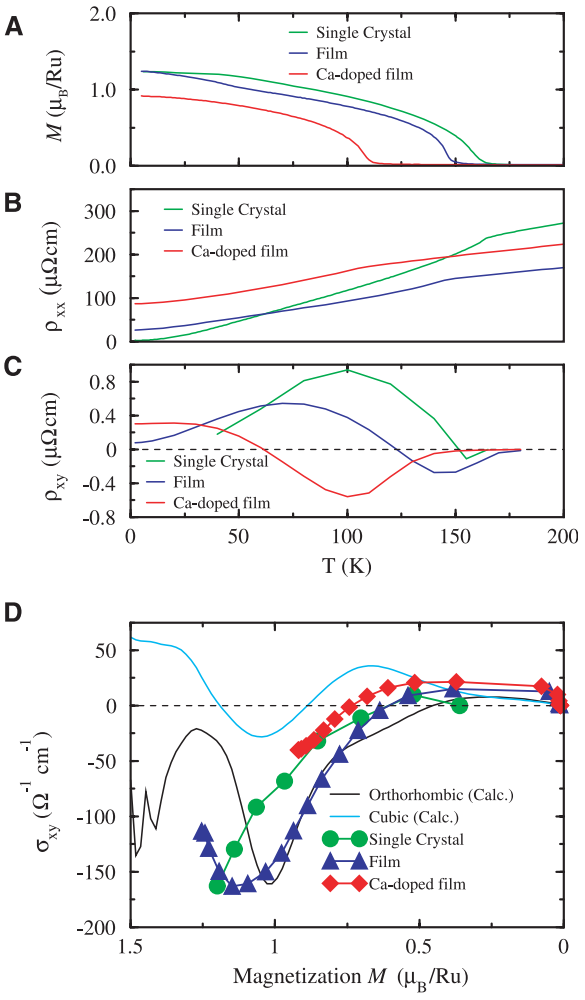

Fig. 1. Measured temperature dependence of the (**A**) magnetization *M*, (**B**) longitudinal resistivity ρ_{xx}, and (**C**) transverse resistivity ρ_{xy} for the single-crystal and thin-film $SrRuO_3$, as well as for the Ca-doped $Sr_{0.8}Ca_{0.2}RuO_3$ thin film. μ_B, Bohr magneton. (**D**) The corresponding transverse conductivity σ_{xy} is shown as a function of *M*, together with the results of first-principles calculations for cubic and orthorhombic structures (*25*). In our calculations, the change of magnetization is taken into account by the rigid splitting of up and down spin bands. As σ_{xy} should vanish with *M* at high temperatures, the calculated σ_{xy} is multiplied by the additional M/M_0 (where $M_0 = 1.5\mu_B$) factor, which does not affect its behavior except in the vicinity of T_c.

$\Sigma_{\mu = 0,1,2,3} f_\mu(\mathbf{k})\sigma_\mu$ where $\sigma_{1,2,3}$ are the Pauli matrices and σ_0 is the unit matrix. When $\mathbf{k}$ is mapped to the vector $\mathbf{f}(\mathbf{k}) = [f_1(\mathbf{k}), f_2(\mathbf{k}), f_3(\mathbf{k})]$, then the contribution to σ_{xy} from the neighborhood of this degeneracy region is given by the solid angle $d\Omega_\mathbf{f}$ for the infinitesimal $dk_x dk_y$ integrated over $\mathbf{k}$. Therefore, the gauge flux near the MM, namely, the degeneracy point $\mathbf{f} = \mathbf{0}$, is singularly enhanced (Fig. 3) (supporting online text).

We studied the behavior of σ_{xy} by first-principles calculations (*16*). The calculated density of states is not so different between the cases with and without SOC (Fig. 4A), whereas the σ_{xy} should be very sensitive to the Bloch wave functions and depends on the Fermi-level position and the spin-splitting (magnetization) substantially, as predicted by the discussion above. We determined the behavior of σ_{xy} as a function of the Fermi-level position by using a small broadening parameter for the lifetime δ (70 meV) (Fig. 4B). When the Fermi level was shifted, not only the absolute value but also the sign of σ_{xy} was found to change. The sharp and spiky structures are the natural results of the singular behavior of the MM (Fig. 3). For the case without any shift of Fermi level, we obtained a value of $\sigma_{xy} = -60\ \Omega^{-1}\ \mathrm{cm}^{-1}$, which has the same sign as and is comparable with the experimental value (about $-100\ \Omega^{-1}\ \mathrm{cm}^{-1}$). Such a spiky behavior should also be reflected in the ω-dependent σ_{xy}, especially for the low-energy range with longer lifetime, whereas it should be suppressed at higher activation energies with shorter lifetime. As shown in Fig. 2 for the ω dependence of optical conductivity, the high-energy (>0.5 eV) part, which is dominated by the $p - d$ charge transfer peak, is usual and can be well reproduced by our calculations, whereas the observed peak structure of $\sigma_{xy}(\omega)$ below 0.5 eV is a clear demonstration of the predicted spiky behavior. The spectra below 0.2 eV were not measured because of the technical difficulty, but structure there should be even sharper, because the dc limit $Re(\sigma_{xy}) \approx -100\ \Omega^{-1}\ \mathrm{cm}^{-1}$ has the opposite sign [the $Im(\sigma_{xy})$ at the dc limit should go back to zero]. Such low-energy behavior is well represented by our calculations, providing further evidence for the existence of MMs.

It is straightforward to understand the results of our transport measurement for σ_{xy}. We attribute the temperature (T) dependence of σ_{xy} to that of the magnetization $M(MT)$. As the result of $\mathbf{k}$-space integration over occupied states, the calculated σ_{xy} is nonmonotonous as a function of M (Fig. 1D). With the reduction of spin-splitting, the calculated σ_{xy}, after the initial increase, decreases sharply, then increases and changes sign (becoming positive), and finally decreases again, capturing the basic features of

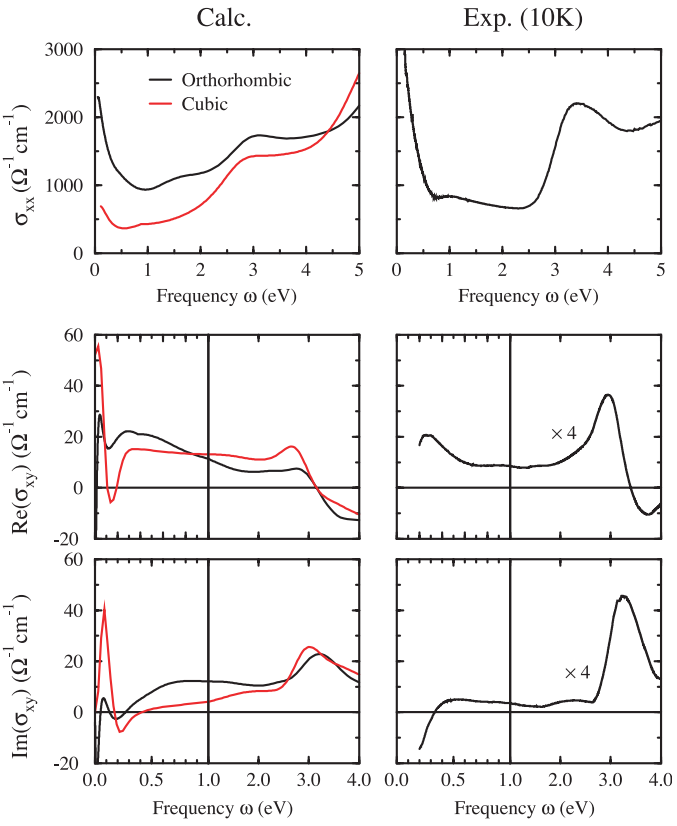

Fig. 2. Calculated (Calc., left panels) and experimental (Exp., right panels) longitudinal (σ_{xx}) and transverse (σ_{xy}) optical conductivity of $SrRuO_3$ film. Measurements were performed at low temperature (10 K). Calculations for both the orthorhombic single-crystal structure and the hypothetical cubic structure kept the average Ru-O bond length. The experimental σ_{xy} values shown are multiplied by a factor of 4. A quantitative comparison of the absolute values of σ_{xy} between the experiments and the calculations would require more accurate structure information. Nevertheless, the clear peak structures for the low-energy σ_{xy} demonstrate monopoles associated with $b_z(\mathbf{k})$.

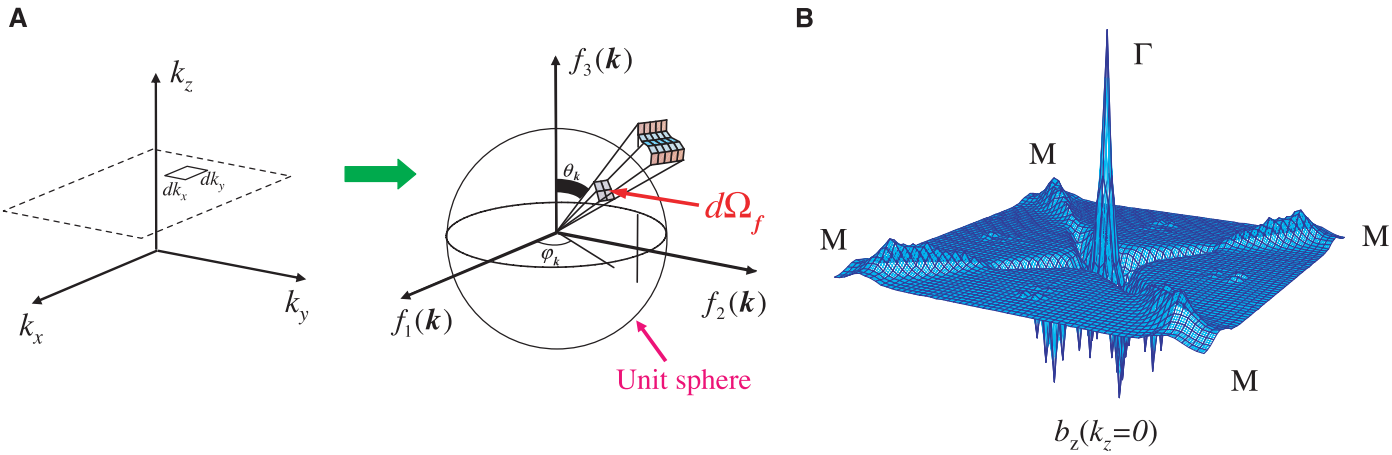

Fig. 3. (**A**) Geometrical meaning of the contribution to σ_{xy} when the two bands are nearly degenerate. The two-dimensional Hamiltonian matrix $H(\boldsymbol{k})$ can be generally written as $H(\boldsymbol{k}) = \Sigma_{\mu = 0,1,2,3} f_\mu(\boldsymbol{k})\sigma_\mu$ where $\sigma_{1,2,3}$ are the Pauli matrices and σ_0 is the unit matrix. When $\boldsymbol{k}$ is mapped to the vector $\boldsymbol{f}(\boldsymbol{k}) = [f_1(\boldsymbol{k}), f_2(\boldsymbol{k}), f_3(\boldsymbol{k})] = f(\boldsymbol{k})(\cos\varphi_{\vec{f}}\ \sin\theta_{\vec{f}},\ \sin\varphi_{\vec{f}}\ \sin\theta_{\vec{f}},\ \cos\theta_{\vec{f}})$, the contribution to σ_{xy} from the neighborhood of this degeneracy region can be given by the $\boldsymbol{f}$-space solid angle $d\Omega_\mathbf{f} = |\delta(\theta_\mathbf{f}, \varphi_\mathbf{f})/\delta(k_x, k_y)|\ \sin\theta_\mathbf{f}\ dk_x\ dk_y = d\varphi_\mathbf{f}\sin\theta d\theta_\mathbf{f}$ for the infinitesimal $dk_x dk_y$ integrated over $\mathbf{k}$. The solid angle corresponds to the flux from the monopole at $\vec{f} = \vec{0}$ (supporting online text). (**B**) Calculated flux distribution in $\vec{k}$ space for t_{2g} bands as a function of (k_x, k_y) with k_z being fixed at 0 for $SrRuO_3$ with cubic structure. The sharp peak around $k_x = k_y = 0$ and the ridges along $k_x = \pm k_y$ are due to the near degeneracy of d_{yz} and d_{zx} bands because of symmetry (supporting online text).

the experimental results. Even more surprisingly, when the measured ρ_{xy} versus T curves shown in Fig. 1C are converted into the σ_{xy} versus M curves shown in Fig. 1D, they now all follow the same trend and match with our calculations. The curves are measured for different samples (with different saturation moments), but all follow the same rule qualitatively and could be simply explained by the reduction of M (*22*) (Fig. 1A). However, the comparison between the experiments and the calculations should be semi-quantitative, because the results are sensitive to the lattice structures. The calculated σ_{xy} for the fictitious cubic structure shows a strong deviation from that obtained for orthorhombic structure, and it changes the sign to be positive at low temperature (at large M). Therefore, more accurate information on the structure is needed to obtain the quantitative result. However, such a sensitivity does not affect our main results, i.e., the nonmonotonous behavior of σ_{xy}. Even the calculations for cubic structure show such behavior and may be used as a guide of possible deviation.

The results and analysis presented here should stimulate and urge the reconsideration of the electronic states in magnetic materials from a very fundamental viewpoint. For example, the MM is accompanied by the singularity of the vector potential, i.e., the Dirac string (*1*). As shown by Wu and Yang (*23*) this means that more than two overlapping regions have to be introduced, in each of which the gauge of the wave function is defined smoothly. This means that one cannot define the phase of the Bloch wave functions in a single-gauge choice when the MM is present in the crystal momentum space. This leads to some nontrivial consequences, such as the vortex in the superconducting order parameter as a function of $\mathbf{k}$ (*24*), and many others are left for future studies.

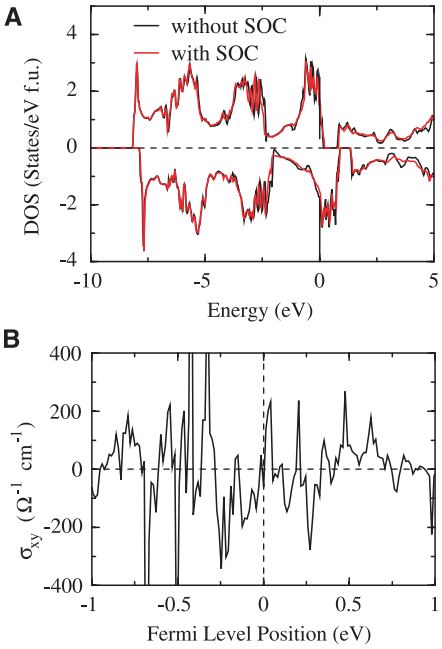

Fig. 4. The calculated (**A**) density of states (DOS) and (**B**) σ_{xy} as functions of Fermi-level position for the orthorhombic structure of single-crystal $SrRuO_3$. The Fermi level is shifted rigidly relative to the converged solution, which is specified as the zero point here. The sharp and spiky structure of σ_{xy} demonstrates the singular behavior of MMs. f.u., the formula unit $SrRuO_3$.

References and Notes

1. P. A. M. Dirac, *Proc. R. Soc. London* **133**, 60 (1931).
2. G. 't Hooft, *Nucl. Phys.* **B79**, 276 (1974).
3. A. M. Polyakov, *JETP Lett.* **20**, 194 (1974).
4. M. V. Berry, *Proc. R. Soc. London Ser. A* **392**, 45 (1984).
5. It has been recognized in the original paper by Berry (*25*) that the degeneracy point in the parameter space acts as a MM where the gauge field is enhanced.
6. H. Ohno, *Science* **281**, 951 (1998).
7. R. Karplus, J. M. Luttinger, *Phys. Rev.* **95**, 1154 (1954).
8. J. Smit, *Physica* **24**, 39 (1958).
9. W. Kohn, J. M. Luttinger, *Phys. Rev.* **108**, 590 (1957).
10. J. M. Luttinger, *Phys. Rev.* **112**, 739 (1958).
11. L. Berger, *Phys. Rev.* **B2**, 4559 (1970).
12. M. Onoda, N. Nagaosa, *Phys. Rev. Lett.* **90**, 206601 (2003).
13. T. Jungwirth, Q. Niu, A. H. MacDonald, *Phys. Rev. Lett.* **88**, 207208 (2002).
14. Y. Taguchi, Y. Oohara, H. Yoshizawa, N. Nagaosa, Y. Tokura, *Science* **291**, 2573 (2001).
15. J. Sinova, T. Jungwirth, J. Kucera, A. H. MacDonald, *Phys. Rev. B* **67**, 235203 (2003).
16. Materials and methods are available as supporting material on *Science* Online.
17. A. Shapere, F. Wilczek, *Geometric Phases in Physics* (World Scientific, Singapore, 1989).
18. D. J. Thouless, M. Kohmoto, M. P. Nightingale, M. den Nijs, *Phys. Rev. Lett.* **49**, 405 (1982).
19. R. M. Martin, *Phys. Rev. B* **5**, 1607 (1972).
20. R. D. King-Smith, D. Vanderbilt, *Phys. Rev. B* **47**, 1651 (1993).
21. This gauge field is distinct from that of the magnetic field $\boldsymbol{B}(\boldsymbol{r})$ in real space, although they are analogous to each other. In the presence of $\boldsymbol{B}(\boldsymbol{r})$, the covariant momentum operator π_μ is given by $\pi_\mu = -i\delta_{z\mu} + eA_\mu(\boldsymbol{r})$ where $\boldsymbol{B} = \nabla \times \boldsymbol{A}$. This leads to the commutation relation $[\pi_x, \pi_y] = -ie(\partial_x A_y - \partial_y A_x) = -ieB_z$, etc., and to the Lorenz force due to the magnetic field $\boldsymbol{B}$. Therefore, these two gauge fields, $b_\mu(\boldsymbol{k})$ and $\mathbf{B}(\mathbf{r})$, are dual to each other, and the presence of the one does not necessarily mean that of the other.
22. More Ca-doped samples with different concentrations have been measured. They all follow the same trend and are not shown here because of space limitations.
23. T. T. Wu, C. N. Yang, *Phys. Rev. D* **12**, 3845 (1975).
24. S. Murakami, N. Nagaosa, *Phys. Rev. Lett.* **90**, 057002 (2003).
25. M. Shikano, T. K. Huang, Y. Inaguma, M. Itoh, T. Nakamura, *Solid State Comm.* **90**, 115 (1994).

Supporting Online Material

www.sciencemag.org/cgi/content/full/302/5642/92/DC1
Materials and Methods
SOM Text
References and Notes

21 July 2003; accepted 28 August 2003

Coherent Soft X-ray Generation in the Water Window with Quasi–Phase Matching

Emily A. Gibson,[1] Ariel Paul,[1] Nick Wagner,[1] Ra'anan Tobey,[1] David Gaudiosi,[1] Sterling Backus,[1] Ivan P. Christov,[2] Andy Aquila,[3] Eric M. Gullikson,[3] David T. Attwood,[3,4] Margaret M. Murnane,[1] Henry C. Kapteyn[1]*

We demonstrate enhanced generation of coherent light in the "water window" region of the soft x-ray spectrum at 4.4 nanometers, using quasi–phase-matched frequency conversion of ultrafast laser pulses. By periodically modulating the diameter of a gas-filled hollow waveguide, the phase mismatch normally present between the laser light and the generated soft x-ray light can be partially compensated. This makes it possible to use neon gas as the nonlinear medium to coherently convert light up to the water window, illustrating that techniques of nonlinear optics can be applied effectively in the soft x-ray region of the spectrum. These results advance the prospects for compact coherent soft x-ray sources for applications in biomicroscopy and in chemical spectroscopy.

Coherent extreme ultraviolet (EUV) and soft x-ray light sources are of interest for applications in lithography, high-resolution imaging, site- and element-specific spectroscopy (*1*), and bio-microscopy (*2–4*). High harmonic generation (HHG) is a useful method for producing coherent, ultrafast, light in this region of the spectrum and can be implemented in a compact setup (*5–11*). In HHG, an intense ultrashort-pulse laser is focused into a gas or solid, generating high harmonics that emerge as a coherent, low-divergence beam (*12*). However, the conversion efficiency of the laser light to shorter wavelengths is limited by

[1]Department of Physics and JILA, University of Colorado, Boulder, CO 80309–0440, USA. [2]Department of Physics, Sofia University, Sofia, Bulgaria. [3]Center for X-ray Optics, Lawrence Berkeley National Laboratory, Berkeley, CA 94720, USA. [4]Applied Science and Technology, University of California, Berkeley, CA 94720, USA.

*To whom correspondence should be addressed. E-mail: kapteyn@jila.colorado.edu